IGSHPA Research Track
Las Vegas, December 6-8, 2022

Uncertainty assessment of the hydraulics properties surrounding a standing column well with a thermal response test

Louis Jacques **Philippe Pasquier**

ABSTRACT

The standing column well (SCW) is known for being a highly efficient ground heat exchanger as it relies on both conduction and advection heat transfer processes. Therefore, the interpretation of a thermal response test (TRT) is strongly influenced both by the hydraulic and thermal properties surrounding the SCW. In this study, it is shown that a TRT can allow identifying the thermal and hydraulic properties around a SCW. The analysis is conducted in a Bayesian framework allowing an accurate and robust identification of the hydraulic properties and their uncertainties. A closed-form expression of the likelihood is used to consider the autocorrelation of the residuals between observed and simulated temperatures. A coupled numerical model is used to generate a training database for an artificial neural network. Then, the latter serves as an emulator of the SCW's short-term g-function given various input parameters. A case study is presented based on a 100-hour TRT performed on a SCW built at a demonstration site located in the city of Mirabel, Canada. For the specific site studied, hydraulic properties were identified with an uncertainty of less than 30 % at a two-sigma level. Such important results lead to more appropriate and efficient design of SCWs.

INTRODUCTION

A ground source heat pump system using SCWs can provide significant energy savings and low peak power usage for buildings (Beaudry *et al.*, 2022). Such ground heat exchangers are also particularly suitable for dense urban areas (Pasquier et al., 2016; Laroche et al., 2022). In a SCW, advective and conductive heat transfer processes are active within the borehole and the geological material surrounding it. Therefore, the design of SCWs requires identifying both thermal and hydraulic properties (Pasquier *et al.*, 2016). To identify hydraulic conductivities, common practice includes hydrogeological investigations, drilling of a test well and pumping tests (Snijders & Drijver, 2016; Beaudry et al., 2018). For the estimation of thermal properties, a TRT can be conducted. For SCWs, estimating the thermal properties with purely conductive models can lead to unrealistic values when hydraulic conductivity is high (Jeon *et al.*, 2016; Robert *et al.*, 2022). However, the interpretation of such a TRT can be done with coupled hydraulic and thermal numerical models (Beaudry *et al.*, 2018; Robert *et al.*, 2022).

Indeed, Robert *et al.* (2022) recently interpreted a TRT in the presence of high hydraulic conductivity (>5x10^{-5} m/s) and obtained a mean absolute error of 0.04 °C between the modelled and measured temperatures. To construct their numerical model, the values of the layered hydraulic conductivity were chosen based on the groundwater cumulative flow observed during drilling and matched with the mean hydraulic conductivity estimated with a pumping test. In this model, the hydrostratigraphic properties are essential to accurately reproduce the measured temperatures (Beaudry *et al.*,

Louis Jacques (louis.jacques@polymtl.ca) is a PhD candidate at Polytechnique Montréal and Philippe Pasquier is a professor of Geological Engineering at Polytechnique Montréal.

DOI: https://doi.org/10.22488/okstate.22.000021

2019). For closed-loop ground-heat exchangers, the identification of hydraulic flux with a thermal response test has been demonstrated in presence of advection. Indeed, interpretation methods have proposed to use the Peclet number to deduce groundwater velocities (Lehr & Sass, 2014; Rouleau *et al.*, 2016) and average hydraulic conductivity (Wagner *et al.*, 2014). Moreover, Lehr & Sass (2014) made use of the groundwater cumulative flow observed during drilling to correlate Peclet number to the thermal conductivity along the profile. Altogether, no TRT interpretation method has yet offered a robust identification of the hydraulic properties around SCWs.

Robustness implies that the methodology employed leads to accurate results, while also dealing with any error it faces. For TRT, errors come from three sources according to Witte (2013). These are measurement errors (instrument precision and resolution), parameter errors (fixed parameters such as borehole length or radius) and model errors (accuracy of the conceptual model itself). For a simple analytical model, an analytical expression of the uncertainty can be used to describe the confidence interval of the variables (Witte, 2013). For more complex mathematical models, Pallard & Lazzarotto (2021) developed a methodology in a stochastic framework taking into account the measurement error and allowing for bias estimation. With a similar goal in mind, Choi *et al.* (2018a) used Bayesian inference to obtain the statistical distributions of unknown thermal properties. Yet, their approach neglected the temporal correlation of the residuals, which is present in temporal series. To solve this problem and accelerate inference, Pasquier & Marcotte (2020) proposed a closed-form equation for the likelihood and an artificial neural network for direct simulations.

In a similar way, this article proposes to use Bayesian inference to assess both the hydraulic and thermal properties surrounding a SCW with TRT data. The methodology used provides the marginal and joint distributions of the properties and, thus, an uncertainty quantification. Since the approach requires millions of simulations, an efficient direct model in the form of a neural network is trained to reproduce the temperatures measured at an experimental SCW. The following sections describe the methodology, an overview of the experimental setup and the main results obtained.

METHODOLOGY

Bayesian Inference

The Bayesian inference framework leads to the marginal and joint distributions of variables θ by drawing from the posterior distribution $P(\theta|x)$ given observations x. In the case of a TRT, these observations are the residuals between the simulated and observed temperatures. The posterior is sampled using a Markov Chain Monte Carlo (MCMC) algorithm which makes use of the simplified Bayes Theorem (Equation 1).

$$P(\theta|x) \propto P(\theta) \cdot P(x|\theta) \tag{1}$$

Prior distributions $P(\theta)$. Firstly, the prior is defined before observations are available. Indeed, a prior reflects an expert judgment of a random variable behaviour. Previously, both Choi *et al.* (2018a) and Pasquier & Marcotte (2020) opted for non-informative uniform priors for all variables. The inference results for these studies showed Gaussian marginal distributions for the thermal properties. Considering these past results, Choi *et al.* (2018b) used triangular prior for the effective thermal conductivity. Again, they obtained marginal distributions following a Gaussian model. On this basis, the present study is using Gaussian distribution as prior, but large standard deviations (σ) are used for each variable. A similar approach was used for hydraulic conductivity as this assumption allows the mean hydraulic conductivity to stay closer to the one deduced from the pumping test.

Likelihood function $P(x|\theta)$. The second step is to evaluate the likelihood function which expresses the probability of making observations conditional to some input properties. The likelihood of the residuals is described by a zero-mean multi-Gaussian distribution which considers temporal correlation, as expressed by Equation (2).

$$P(x|\Theta) = (2\pi)^{-\frac{n}{2}}|\Sigma|^{-\frac{1}{2}}e^{-\frac{1}{2}x'\Sigma^{-1}x} \tag{2}$$

For large covariance matrix (Σ), evaluation of Equation 2 is costly and this work used the exact closed-form solution

proposed by Pasquier & Marcotte (2020) to ease its evaluation. The solution requires modeling the variogram of the residuals and estimation of the variance and correlation range.

Posterior sampling $P(\theta|x)$. To sample the posterior distribution an ensemble slice sampler based on the work of Karamanis & Beutler (2021) and allowing for a parallel and efficient inference was used. The sampler was employed with 50 parallel chains and 100 000 samples per chain. Since the acceptance rate was around 15%, the direct model was called more than 33 million times. A fast and efficient direct model is therefore required to complete the inference in a realistic time frame.

Direct Model and Training Database

A coupled numerical model was constructed within the Comsol Multiphysics environment (Comsol*,* 2022) to simulate groundwater flow and heat transfer. This model was used to assemble a training database that was used later to train an artificial neural network (ANN) designed to construct the short-term g-function of the SCW. The numerical modelling strategy is the same as the one described by Beaudry *et al.* (2019). An axisymmetric model is used to represent the SCW with the center of the well located on the symmetry axis. Table 1 presents the main components of the numerical model as reported by Robert *et al.* (2022) for the study site. The thermal conductivities of the subsurface materials ($k_{s,i}$) and the hydraulic conductivities of the hydrostratigraphic layers ($K_{h,j}$) are variable in the inference. The thermal boundary conditions are composed of a null heat flux at the bottom of the model and a constant temperature at the surface and at the far field. These boundary conditions are based on the quasi-constant temperature observed in the wells during three different thermal profile logging. Regarding the hydraulic boundary conditions, flow was restricted at the bottom and top of the model and a constant hydraulic head was applied at the far-field limit to represent the fact that groundwater was 2.5 m deep. Finally, the groundwater flow was simulated under a steady state since a long continuous circulation phase is conducted in the TRT before heat injection.

Table 1. Numerical model main components for the SCW and subsurface materials

Parameter	Units	Water/Well	HDPE	Till	Sandy dolomite	Quartz arenite
Thickness (b)	m	133.20	0.00549	10.05	89.01	34.14
Diameter	m	0.152	0.0493 /0.0603	150*	150*	150*
Porosity	%	-	0.001	20	2.2	5.9
Volumetric heat capacity (C)	MJ/(m^3 K)	4.18	2.28	2.30	2.31	2.18
Thermal conductivity (k)	W/(m K)	0.56	0.42	θ	θ	θ

*This diameter represents the extension of the axisymmetric numerical model.

Artificial Neural Network and Simulation Approach

The numerical model exploits an optimized mesh and efficient solver. However, computation of the g-functions is still long for the current purpose of this study. Indeed, every call of the numerical model requires more than a minute and the inference process would converge after multiple years of computation. To accelerate the inference, an ANN inspired from Pasquier et al. (2018) and Pasquier & Marcotte (2020) was used as a surrogate model. The ANN architecture includes 10 hidden layers with 50 neurons each and an output layer of 95 neurons. The input layer is composed of seven parameters (θ) and nine enriched parameters (ψ), chosen to accelerate network training. Here, these parameters are the thermal diffusivity (α=k/C), hydraulic transmissivity (K·b) and the weighted average of k and K ($\overline{k}$ and $\overline{K}$). Table 2 summarizes these parameters. Before training the ANN, a transformation is applied to the short-term g-function as it also helps the training process. Moreover, a normalization between -1 and +1 is applied to all input and output.

Table 2. Training parameters (θ) and enriched parameters (ψ)

Parameter	Till	Sandy dolomite	Quartz arenite	Hydrostratigraphic layers			
θ	$k_{s,1}$	$k_{s,2}$	$k_{s,3}$	$K_{h,2}$	$K_{h,3}$	$K_{h,4}$	$K_{h,5}$
ψ	$\alpha_{s,1}$	$\alpha_{s,2}$	$\alpha_{s,3}$	$K_{h,2}\cdot b_{h,2}$	$K_{h,3}\cdot b_{h,3}$	$K_{h,4}\cdot b_{h,4}$	$K_{h,5}\cdot b_{h,5}$
	$\bar{k}$ (weighted average)			$\bar{K}$ (weighted average)			

The ANN directly provides the g-function corresponding to the entering water temperature (EWT) at the TRT unit (Figure1 a)). Then, the leaving water temperature (LWT) signal is obtained efficiently using fast Fourier transforms (see Marcotte & Pasquier, 2008, Pasquier et al. 2018) through:

$$LWT(t) = T_{i=0} + (f * g)(t) + \Delta T(t) \tag{3}$$

where g is the short-term g-function and f is the excitation function specified by Equation (4).

$$f(t) = \Delta T(t_i) - \Delta T(t_{i-1}) = \frac{\dot{Q}(t_i) - \dot{Q}(t_{i-1})}{\dot{v}\, c} \tag{4}$$

Experimental Case Study

A TRT was conducted at an experimental site located in the city of Mirabel, Québec. The study site is described in detail by Robert *et al.* (2022). Figure 1 a) presents the TRT unit connected to the SCW. The TRT unit includes monitoring of the entering and leaving water temperature (EWT and LWT). For their base case, Robert *et al.* (2022) demonstrated an optimal fit of temperatures with specific values of thermal and hydraulic conductivities. Figure 1b) shows these base case values for the thermal conductivity varying according to the three subsurface materials. Figure 1c) shows the

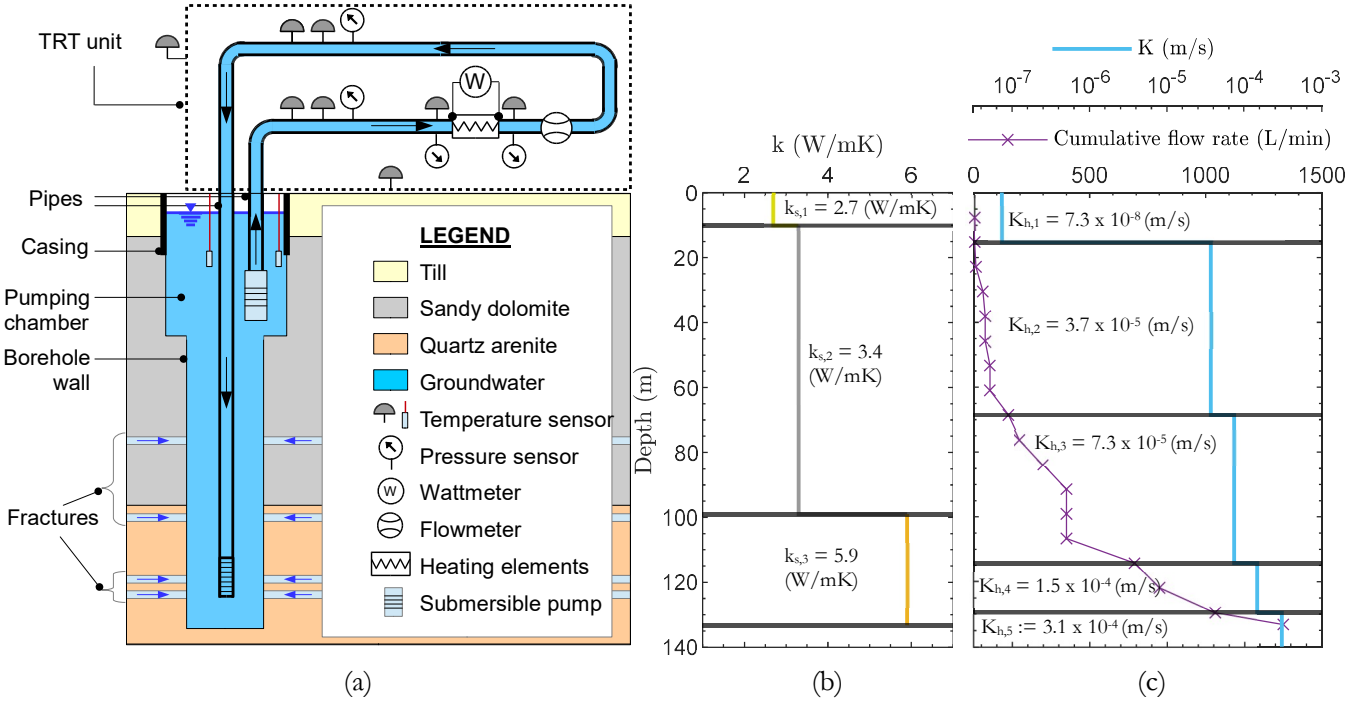

Figure 1 a) Stratigraphy, experimental SWC and TRT unit. b). Stratigraphy and base case values of thermal conductivity ($k_{s,i}$ for i=1, 2 and 3) for each subsurface materials. c) Hydrostratigraphy, groundwater flow rates observed during drilling and base case values of hydraulic conductivity ($K_{h,j}$ for j=1,2,3,4 and 5) for each hydrostratigraphic layers is shown in pale blue.

hydraulic conductivity following the five different hydrostratigraphic units (light blue). These hydrostratigraphic units are based on the variation of groundwater flow regime in the materials and their delimitation is independent of the nature of these materials. This hydraulic conductivity profile matches the groundwater cumulative flow observed while drilling and the mean value of 6.5x10^{-5} m/s obtained by the pumping test (Robert et al., 2022). Also, Figure 1c) illustrates groundwater cumulative flow rates observed while drilling.

Figure 2 (upper left) presents the observed LWT during the TRT and the simulated temperatures. The temperature variation ΔT is used to evaluate the excitation function *f(t)* shown on the right axis. This TRT is separated in two phases. The first one is a continuous circulation phase that lasted for approximately 18 hours. Afterwards, the heating phase was started and lasted 83 hours. During this phase, the heating elements were powered at around 21 kW. Figure 2 (lower left) presents the residuals between simulated and observed temperatures during the heating phase. Note that the first 4.67 hours were discarded. Indeed, the circulation pump was interrupted for 103 minutes prior to the heating phase and fitting the model to the data was more difficult at the onset of the TRT. Finally, Figure 2 (right) shows the variogram corresponding to the optimal residuals as obtained by a single multidimensional optimization. The variogram has a

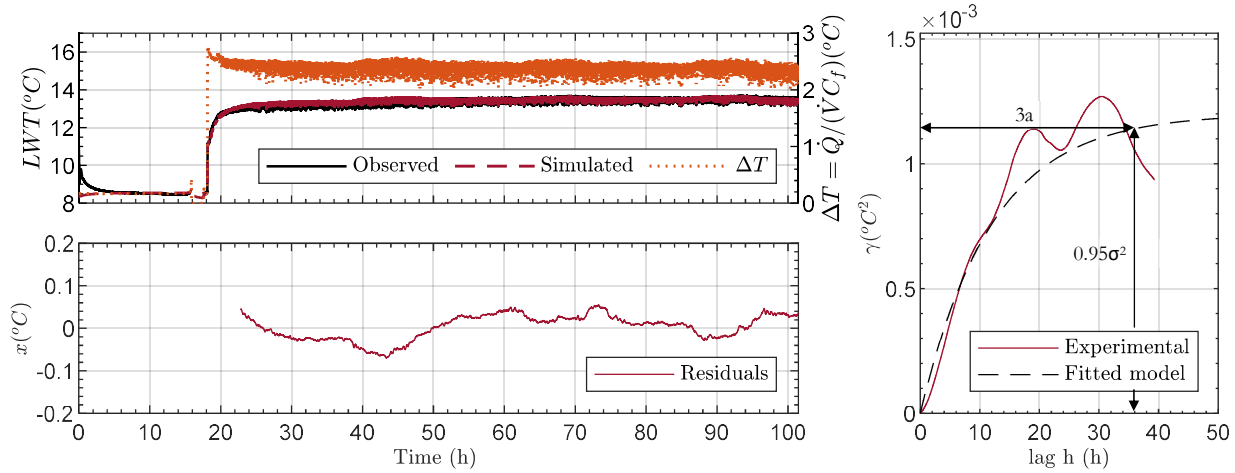

Figure 2 Upper left: Observed and optimal simulated leaving water temperatures used to compute residuals *x* and temperature variation ΔT used to compute excitation function *f*. Bottom left: temperature residuals used to compute experimental variogram. Right: experimental variogram *(γ)* and fitted covariance model.

variance of σ^2 = 1.2 x 10^{-3} °C^2 and a correlation range of a = 12 h.

RESULTS AND DISCUSSION

A Bayesian inference was conducted using the parameters of the experimental variogram to evaluate the likelihood. Gaussian priors were set for the three subsurface thermal conductivities ($k_{s,i}$ for i=1, 2 and 3) and for the four deepest hydraulic conductivities ($K_{h,j}$ for j=2 to 5). Indeed, the first hydrostratigraphic layer is not inferred as this layer is sealed with a casing for most of its depth. Hence, we observed that this layer's hydraulic conductivity has no significant influence on the evolution of EWT.

The Bayesian inference is completed with a posterior distribution of 100 000 samples for each of the 50 chains, for a total of 5 million samples. The acceptance rate reached 14.4 %, resulting in a total of 34.7 million simulations and a computation time of approximately 116 hours. A burn-in period of 50 000 samples per chain was used to analyze the marginal and joint distributions. Accordingly, Figure 3 presents these distributions, along with a scatter plot showing the correlation between each pair of variables. On the diagonal, the marginal samples are plotted in orange, while the green line corresponds to the prior distributions. As an indication of the success of the inference, the mean absolute

error of the corresponding residuals stands between 0.02 ºC and 0.04 ºC (at a two-sigma level). These results correspond to the mean absolute error (MAE) of 0.04 ºC obtained by Robert *et al.* (2022) for their base case and which correspond to the vertical black lines in Figure 3.

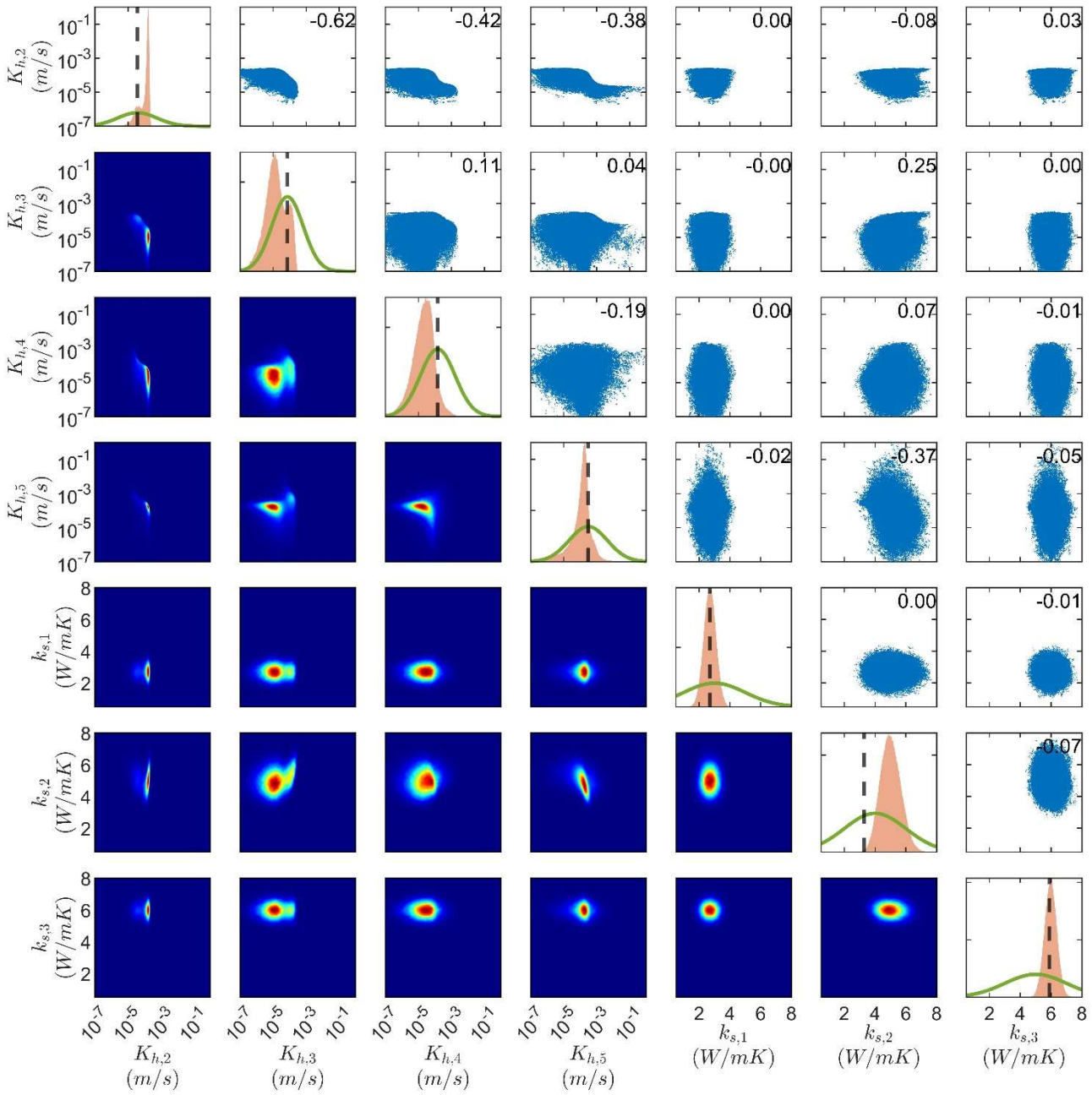

Figure 3 - Marginal (diagonal) and joint (lower triangle) distributions of the hydraulic conductivity of the four deepest hydrostratigraphic layers ($K_{h,i}$ for j=2, 3, 4 and 5) and thermal conductivity of the different subsurface materials ($k_{s,i}$ for i=1, 2 and 3). Scatter plots and correlation (upper triangle). On the diagonal, the Gaussian prior are drawn in green and the dashed black lines represents the base case values from Robert *et al.* (2022).

The most striking result is the fact that inferred distributions are all well defined Gaussian-like distributions and all significantly differ from their priors. Even more interesting is the fact that the mean hydraulic conductivity obtained in this work is almost the same as the one obtained by a pumping test. Indeed, Figure 4 a) presents the weighted average for all samples of K using the unit's thickness *b* as weight. The mean value inferred is 7.5 x 10^{-5} m/s while a value of 6.5 x 10^{-5} m/s was obtained with a pumping test, leading to a difference of +1.5 % of their logarithmic value. Therefore, inferring hydraulic properties with a TRT is feasible and can be done with great accuracy.

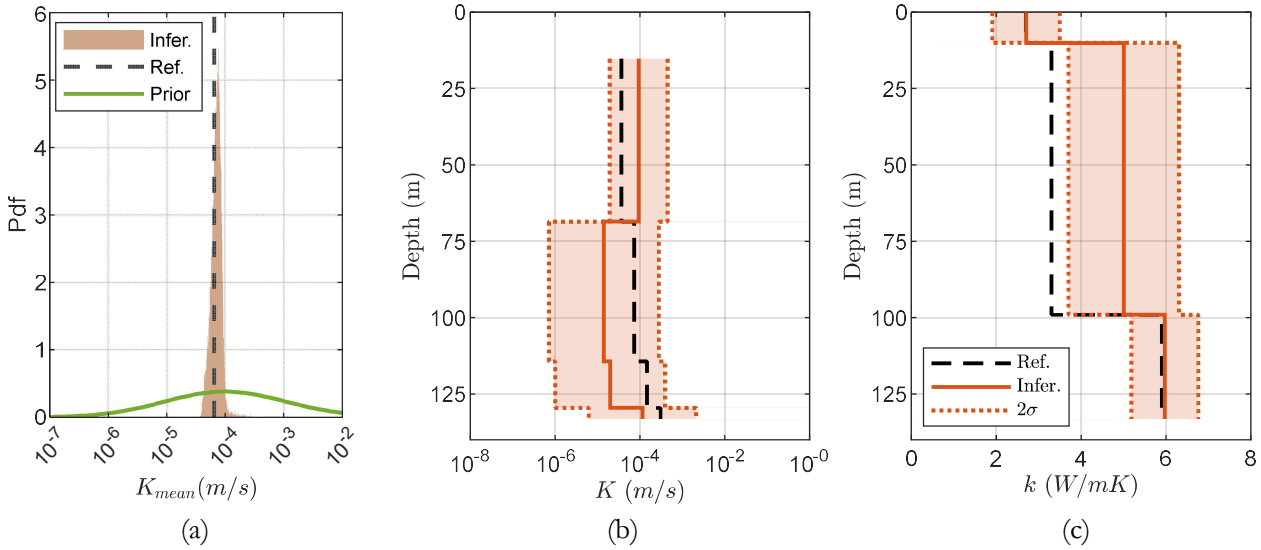

Figure 4 - a) Weighted average of the hydraulic conductivities. Values obtained by inference (orange), by a pumping test (black) or given by the prior (green). b) Mean hydraulic conductivties for each hydrostratigraphic unit and c) and thermal conductivity of subsurface materials and their uncertainties at a two-sigma level.

Figure 4b) presents a comparison with the reference case from Robert *et al.* (2022) for the inferred hydraulic conductivities. The mean values of the marginal distributions for the three deepest units are all inferior (orange dashed line) to the reference case, while the value of the second layer is higher. Thus, the inferred mean values observed on Figure 4b) contradict the pattern of the reference case that was based on the cumulative groundwater flow observed during drilling (see Figure 1). In fact, these drilling observations are prone to increasing error as the cumulative flow rise. This is somehow illustrated by the fact that confidence interval for the hydraulic conductivities increases with depth with values of 6 %, 18 %, 19 % and 22 %. Even so, all hydraulic conductivities from the reference case are within the uncertainty of the inferred hydraulic conductivities.

For the thermal conductivities, Figure 4c) indicates that the values of the first and last subsurface materials are unchanged in comparison with the reference case. However, the value inferred for the sandy dolomite ($k_{s,2}$) reached 5.0 W/(mK) in contrast with expected value of 3.4 W/(mK), leading to a difference of 47 %. It should be noted, however, that the value of 3.4 W/(mK) comes from a laboratory test performed on a rock sample gathered a few kilometers from the study site. To finish, we mention that as reported by Jeon *et al.* (2016), it is difficult to obtain accurate thermal conductivity in a context of high hydraulic conductivity (>5x10^{-5} m/s).

CONCLUSION

In this paper, a methodology is proposed to infer hydraulic conductivities and their uncertainties with a thermal response test (TRT) conducted on a standing column well (SCW). In a Bayesian framework, the computation of likelihood is completed considering residuals between measured and simulated temperatures. To ease the evaluation of the likelihood, an exact closed-form solution of the likelihood is employed. The temperature is simulated with an artificial neural network mimicking a numerical model that couples heat transfer and groundwater flow. A case study presents a TRT conducted on a SCW. High cumulative groundwater flows were observed during drilling. Thus, advective heat transfer plays an important role for this case study. Using Bayesian inference, it was shown that identification of hydraulic properties is possible with a thermal test. The average hydraulic conductivity inferred has a diffrence of 1.5 % in comparison with the results of a pumping test conducted on the same SCW. Moreover, the highest confidence interval reached 22 % for the hydraulic properties.

ACKNOWLEDGMENTS

The authors acknowledge the support from partners of the Geothermal Research Chair on the Integration of SCWs in Institutional Buildings, namely Hydro-Québec, the Ministry of higher education of Québec, CSSMI, CSSDM, CSSS, Versa Profiles, Marmott Energy, CanmetEnergy and NSERC. Additionally, we thank the anonymous reviewers and colleagues (A. Courchesne and M. Arbi Ben Aoun) that provided constructive comments. This work was financed by the Natural Sciences and Engineering Research Council of Canada through grant number ALLRP 544477-19.

NOMENCLATURE

α	=	thermal diffusivity (m^2/s)
b	=	thickness (m)
C	=	volumetric heat capacity ($J/(m^3K)$)
f	=	excitation function (°C)
g	=	short term g-function (-)
γ	=	variogram function ($units^2$)
φ	=	diameter (m)
k	=	thermal conductivity (W/(mK))
K	=	hydraulic conductivity (m/s)
n	=	number of residuals (-)
P	=	probability
$\dot{Q}$	=	heating power (W)
σ	=	standard deviation
T	=	temperature (°C)
Θ	=	parameters
ψ	=	enriched parameters
x	=	temperature residuals (°C)
$\dot{V}$	=	circulation flow rate (m^3/s)

Subscripts

b	=	hydrostratigraphic layer
s	=	subsurface layer

REFERENCES

Beaudry, G., Pasquier, P., and D. Marcotte. 2018. *Hydrogeothermal characterization and modelling of a standing column well experimental installation*. Proceedings of the IGSHPA Research Track 2018, 1–10.

Beaudry, G., Pasquier, P., and D. Marcotte. 2019. *The impact of rock fracturing and pump intake location on the thermal recovery of a standing column well: Model development, experimental validation, and numerical analysis*. Science and Technology for the Built Environment, 25(8)

Beaudry, G., Pasquier, P., Marcotte, D., and A. Zarrella. 2022. *Flow rate control in standing column wells: A flexible solution for reducing the energy use and peak power demand of the built environment*. Applied Energy, 313, 118774.

Choi, W., Kikumoto, H., Choudhary, R., and R. Ooka. 2018. *Bayesian inference for thermal response test parameter estimation and uncertainty assessment*. Applied Energy, 209, 306–321.

Choi, W., Menberg, K., Kikumoto, H., Heo, Y., Choudhary, R., and R. Ooka. 2018. *Bayesian inference of structural error in inverse models of thermal response tests.* Applied Energy, 228, 1473–1485.

Comsol A.B. 2022. *COMSOL Multiphysics v. 6.0.*, Stockhol; Sweden.

Jeon, J.-S., Lee, S.-R., and W.-J. Kim. 2016. *Applicability of thermal response tests in designing standing column well system: A numerical study.* Energy, 109, 679–693.

Karamanis, M., and F. Beutler. 2021. *Ensemble Slice Sampling: Parallel, black-box and gradient-free inference for correlated & multimodal distributions.* ArXiv:2002.06212 [Astro-Ph, Stat].

Laroche, V., Pasquier, P., and B. Courcelles. 2022. *Integration of standing column wells in urban context: A numerical investigation-case in the City of Montreal.* Sustainable Cities and Society, 78, 103513.

Lehr, C., and I. Sass. 2014. *Thermo-optical parameter acquisition and characterization of geologic properties: A 400-m deep BHE in a karstic alpine marble aquifer.* Environ Earth Sci, 17.

Marcotte, D., and P. Pasquier. 2008. *Fast fluid and ground temperature computation for geothermal ground-loop heat exchanger systems.* Geothermics, 37(6), 651–665.

Pallard, W. M., and A. Lazzarotto. 2021. *Thermal response tests: A biased parameter estimation procedure?* Geothermics, 97, 102221.

Pasquier, P., and D. Marcotte. 2020. *Robust identification of volumetric heat capacity and analysis of thermal response tests by Bayesian inference with correlated residuals.* Applied Energy, 261, 114394; 1–18.

Pasquier, P., Nguyen, A., Eppner, F., Marcotte, D., and P. Baudron. 2016. *10—Standing column wells.* In S. J. Rees (Ed.), Advances in Ground-Source Heat Pump Systems (pp. 269–294). Woodhead Publishing.

Pasquier, P., Zarrella, A., and R. Labib. 2018. *Application of artificial neural networks to near-instant construction of short-term g-functions.* Applied Thermal Engineering, 143, 910–921.

Robert, S., Pasquier, P., and A. Nguyen. 2022. *Impact of layered heterogeneity on thermal response test interpretation performed on a standing column well operated without bleed.* Geothermics, 101, 102353.

Rouleau, J., Gosselin, L., and J. Raymond. 2016. N*ew concept of combined hydro-thermal response tests (H/TRTS) for ground heat exchangers.* Geothermics, 62, 103–114.

Snijders, A. L., and B. C. Drijver. 2016. *9—Open-loop heat pump and thermal energy storage systems*. In S. J. Rees (Ed.), Advances in Ground-Source Heat Pump Systems (pp. 247–268). Woodhead Publishing.

Wagner, V., Bayer, P., Bisch, G., Kübert, M., and P. Blum. 2014. *Hydraulic characterization of aquifers by thermal response testing: Validation by large-scale tank and field experiments.* Water Resources Research, 50(1), 71–85.

Witte, H. J. L. 2013. *Error analysis of thermal response tests.* Applied Energy, 109, 302–311.